Available online at www.sciencedirect.com

ScienceDirect

Transportation Research Procedia 91 (2025) 632–639

Transportation Research Procedia

www.elsevier.com/locate/procedia

The Science and Development of Transport - TRANSCODE 2025

Optimization of Flexible Pavement Layer Composition Considering Fatigue and Rutting Distresses

Ali Pirdavani[a,b,*], Bram Huybrecht[a], Bram Truyers[a], Thomas Van de Velde[a]

[a]*UHasselt, Faculty of Engineering Technology, Agoralaan, Diepenbeek 3590, Belgium*
[b]*UHasselt, The Transportation Research Institute, Martelarenlaan 42, Hasselt 3500, Belgium*

Abstract

This study investigates the impact of pavement layer and material composition on the structural durability of flexible road surfaces, focusing on fatigue cracking and rutting resistance. Based on Flemish Class B6 roads, eight pavement design scenarios were modeled using 3D-Move Analysis software under static triple-axle truck loading conditions. Variations included surface materials (SMA-C, ZOA-B), asphalt layer thickness, and base stabilization methods (cement, lime, or unbound). Results demonstrate that cement-stabilized crushed stone bases significantly outperform lime-treated and unbound stone bases, reducing rutting and fatigue strain values. Fatigue damage was most influenced by horizontal strains at the bottom of the asphalt layers, while rutting correlated with vertical strains in the base layer. Cement-bound bases showed up to 36 times longer fatigue life and 54% better rutting resistance compared to unbound stone. Although surface layer properties had a secondary effect, minor material changes could still shift performance by hundreds of thousands of load repetitions. The findings underline the dominant role of base layer treatment in enhancing pavement longevity and advocate for the inclusion of cement-stabilized bases in future sustainable road designs.

Keywords: 3D-Move Analysis; fatigue cracking; flexible pavement; pavement layer composition; rutting

1. Introduction

Repeated traffic loading significantly deteriorates road structures, primarily through fatigue cracking and rutting. Fatigue cracking occurs when traffic-induced stresses exceed the material's fatigue limit, leading to structural failure and water infiltration. Rutting results from permanent deformation due to weak compaction, excessive stress, or soft

* Corresponding author. Tel.: +32 11 29 2183
E-mail address: ali.pirdavani@uhasselt.be

2352-1465
10.1016/j.trpro.2025.10.081

asphalt, particularly under high temperatures. Elnashar et al. (2019) and Asim et al. (2021) state these issues compromise safety, vehicle maneuverability, and pavement longevity. This study aims to improve the durability of flexible pavement structures by analyzing how material properties and layer configurations influence resistance to fatigue and rutting. In Flanders, pavement design follows a classification system known as *bouwklassen*, ranging from B1 (high-capacity highways) to B9 (low-volume access roads). For each class, multiple standard pavement layer compositions are permitted. However, current guidelines provide limited performance-based comparison between these options, leaving designers without clear evidence to support one layout over another.

Previous research has extensively explored pavement response under repeated loading using empirical and mechanistic-empirical approaches. Finite element tools have been employed to simulate pavement layer behavior under axle loads, like in Kumar et al. (2024) and Liu et al. (2025). Studies have investigated how variations in material stiffness, thickness, and sublayer characteristics influence pavement performance indicators like fatigue cracking and rutting. However, few works have focused on performance-based comparisons among standardized pavement compositions within existing regional frameworks. In particular, limited attention has been given to the Flemish *bouwklassen* system, where multiple design options are allowed per class but without accompanying quantitative guidance. This study addresses that gap for Class B6 roads by offering a comparative analysis based on mechanical response and relative performance under consistent loading conditions.

The study focuses on Class B6 as a representative mid-level construction class commonly used for regional roads that experience moderate but non-negligible traffic volumes. B6 roads are critical to the Flemish network because they often serve as connectors between local and arterial roads, and they are frequently subject to structural degradation due to mixed traffic loads. This makes them an ideal case for investigating the trade-offs between different standard pavement configurations in terms of long-term performance. Using eight design scenarios based on Flemish Class B6 road construction standards (with Type 1 subbase), the study varies pavement layer composition, dimensions, density, and E-modulus to assess structural performance. The key innovation lies in translating design standards into quantifiable performance indicators, allowing practitioners to compare and select among existing configurations based on expected resistance to fatigue and rutting. The ultimate goal is to support the development of longer-lasting pavements with reduced maintenance demands, thereby minimizing traffic disruptions and environmental impact. By providing data-driven insights into how pavement structure and material behavior contribute to damage progression, this research advances both practical design decisions and broader goals for sustainable infrastructure.

2. Methods and materials

2.1. Materials and Scenarios

The layer composition and materials of flexible pavements significantly affect fatigue cracking and rutting, as Singh et al. (2018) demonstrated. A typical structure includes four layers: subgrade, subbase, base, and bituminous layers. In this study, the subgrade consists of soil, and the subbase uses Type 1 material based on Flemish road construction guidelines. The base layer is an unbound crushed stone, analyzed both in its original form and with cement or lime additives, as it plays a crucial role in distributing traffic loads, as stated by the Pavement Tools Consortium (2025).

The bituminous surface consists of a base course (APO-A) and a wearing course, either Stone Mastic Asphalt Class C (SMA-C) or Very Open Asphalt Type B (ZOA-B), outlined in the 'Vademecum Standaardstructuren' (2023). ZOA is highly rut-resistant, while SMA is slightly more susceptible; both are common on heavily trafficked roads. The suffix (e.g., SMA-C) indicates nominal aggregate size: APO-A = 0/20 mm (Type A), ZOA-B = 0/14 mm (Type B), SMA-C = 0/10 mm. SMA and ZOA are stone skeleton mixtures ($\geqslant$70% coarse aggregate), enabling load transfer through stone-to-stone, as highlighted by Devree (2025). Key parameters—E-modulus, Poisson's ratio, density, unit weight, and damping ratio—were collected for all layers and are listed in Table 1, based on information retrieved from 'Standaardbestek 250' (2019), Pirdavani et al. (2023), Yeganeh et al. (2023), and Ullah et al. (2024).

Eight pavement scenarios were developed, differing in material composition and asphalt layer thickness. These scenarios were defined based on the 'Vademecum Standaardstructuren' (2023) and 'Standaardbestek 250' (2019), which provide the official guidelines for flexible pavement design in Belgium. A preliminary assessment indicated that most configurations could be effectively modeled using a Type B6 structure, representing a wide range of local

and provincial roads. This class allows combinations of different surface layers with various APO-A thicknesses. The specific layer compositions and thicknesses used in each scenario are summarized in Table 2.

Table 1. Pavement parameters.

	Bituminous layers			Base			Subbase	Subgrade
Linear Elastic Materials	SMA-C	ZOA-B	APO-A	Cement	Lime	Stone		
E-modulus (MPa)	3000	2800	2500	1400	600	400	250	50
Poisson ratio (-)	0.35	0.35	0.35	0.25	0.25	0.25	0.35	0.3
Density (kg/m³)	2290.93	2051.99	2417.94	2400.00	1800.00	2100.00	1936.80	1834.86
Unit Weight (kN/m³)	22.47	20.13	23.72	23.54	17.66	20.60	19.00	18.00
Damping Ratio (%)	4	5.5	5	0.8	0.8	3	7.5	10.5

Table 2. Layer composition and thicknesses of the eight pavement design scenarios.

Scenario	Surface Layers (cm)	Base Type	Base (cm)	Subbase (cm)	Subgrade soil (cm)
1	SMA-C (4), APO-A (6), APO-A (6)	Stabilized crushed stone (cement)	25	39	500
2	ZOA-B (4), APO-A (6), APO-A (6)	Stabilized crushed stone (cement)	25	39	500
3	SMA-C (4), APO-A (7), APO-A (8)	Stabilized crushed stone (lime)	25	36	500
4	SMA-C (5), APO-A (7), APO-A (7)	Stabilized crushed stone (lime)	25	36	500
5	ZOA-B (4), APO-A (7), APO-A (8)	Stabilized crushed stone (lime)	25	36	500
6	SMA-C (4), APO-A (8), APO-A (8)	Unbound crushed stone (unstabilized)	35	25	500
7	SMA-C (5), APO-A (7), APO-A (8)	Unbound crushed stone (unstabilized)	35	25	500
8	ZOA-B (4), APO-A (8), APO-A (8)	Unbound crushed stone (unstabilized)	35	25	500

2.2. Used Software – 3D-Move Analysis

The simulations were performed using 3D-Move Analysis, a software tool based on a continuum-based finite-layer method. Applying Fourier transform techniques enables efficient and accurate analysis of complex surface loading conditions that are particularly suitable for horizontally layered pavement structures.

A static analysis was conducted using a triple-axle configuration with single tires, where each tire was modeled with a circular contact footprint. This setup reflects the typical loading pattern of heavy trucks. The choice for a triple-axle configuration was deliberate, as trucks impose significantly higher axle loads than passenger vehicles, allowing for a more conservative and realistic assessment of pavement performance and damage progression under real-world traffic conditions.

The total axle load of 21,000 kg, based on the Belgian legal limit, corresponds to a force of 206.01 kN divided over six tires, resulting in a wheel load of 34.34 kN per tire. A tire pressure of 500 kPa was applied, a rolling friction coefficient of 0.3 was used, and the vehicle suspension was configured as "no DLC", meaning no dynamic load compensation was applied, reclaimed from Transport Friends (2025).

2.3. Empirical models for fatigue cracking and rutting

Based on the data obtained from the simulations, this section elaborates on the mathematical formulations applied in the subsequent analysis. These empirical models estimate the allowable load repetitions, as Behiry (2012) prescribes. To ensure the calculations are consistent with Belgian engineering practice, the models incorporate region-specific coefficients provided by the Belgian Road Research Center (BRRC). In this study, the coefficients relevant to fatigue analysis (i.e., f_1=4.92E-14, f_2=4.76, and f_3=0) and those used in the rutting calculations (i.e., f_4=3.05E-09 and f_5=4.35) are utilized based on the corresponding BRRC-recommended values.

The number of allowable load repetitions before fatigue cracking initiation is calculated using the following general equation:

$$N_f = f_1 \times \epsilon_t^{-f_2} \times E_1^{-f_3} \quad (1)$$

In this equation, N_f denotes the allowable number of load cycles before fatigue failure. The variable ε_t is the horizontal tensile strain at the bottom of the asphalt layer obtained from simulation results. E_1 represents the asphalt's elastic modulus. The BRRC assumes that the modulus has negligible influence by setting the coefficient f_3 hitherto zero. Similarly, the formula for allowable load repetitions before rutting becomes critical is:

$$N_r = f_4 \times \left(\frac{1}{\varepsilon_v}\right)^{f_5} \quad (2)$$

Here, N_r represents the allowable number of load applications before rutting failure. ε_v is the vertical compressive strain at the top of the subgrade. These equations form the basis for evaluating pavement performance and the long-term durability of the construction scenarios in this study.

3. Results

Normal strains were analyzed in three directions: vertical (Z-Z), longitudinal (X-X), and transverse (Y-Y). Z-Z strains were used to assess rutting, while X-X and Y-Y indicated fatigue. Empirical models estimated pavement service life. Five measurement points were defined within the tire footprint for each of the three-wheel positions—X-coordinates fixed per wheel and Y-coordinates spaced at 7.4 cm intervals. The maximum strain from these five points was used for further analysis.

3.1. Rutting

Positive strain values indicate compressive deformation in the subgrade and base layers for rutting, accumulating over time under repeated loads. This leads to asphalt flow and upward deformation along the wheel path, known as uplift rutting. Simulations provided Z-Z strain values for eight scenarios, all at the top of the subgrade layer (i.e., depth of 80 cm for all scenarios). For each tire footprint, a maximum of five measurement points—usually at the tire center—were used for comparison. These peak values are shown in Fig. 1.

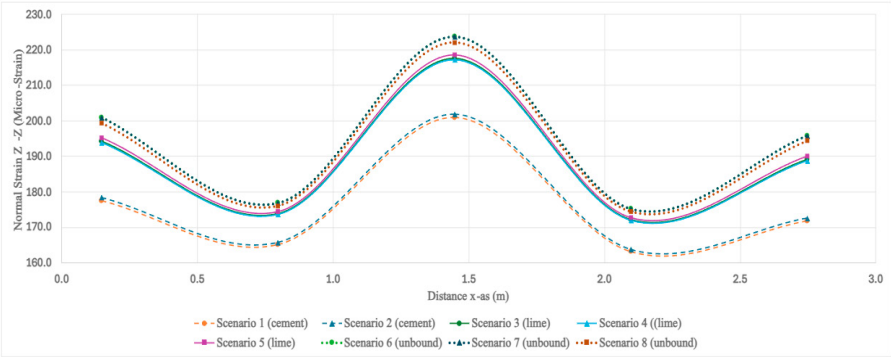

Fig. 1. Normal strains in Z-Z direction.

Fig. 1 presents Z-Z strain versus X-position for all scenarios, grouped by base material: Group 1 (scenarios 1–2, cement-stabilized), Group 2 (scenarios 3–5, lime-stabilized), and Group 3 (scenarios 6–8, unbound crushed stone). Group 1 showed the lowest strain values, and Group 3 the highest. All scenarios followed a similar trend: two minima between tires and a peak under the second wheel. Minor modeling deviations explain the small differences between tires 1 and 3. The strain was always lowest at the tire edges and highest at the center.

3.2. Fatigue cracking

For fatigue analysis, negative strain values indicate tensile strain—critical for crack initiation—while positive values indicate less damaging compressive strain. Fatigue was assessed using X-X and Y-Y strains at 16, 19, or 20

cm depth, depending on the base layer, representing the bottom of the asphalt. A maximum of five measurement points per tire, usually at the tire center, was used. Peak Y-Y strain values along the X-axis are shown in Fig. 2. The graphs show scenario clusters based on base material: scenarios 1 and 2 (cement-stabilized) had significantly lower absolute strains than scenarios 3–5 (lime-stabilized), while scenarios 6–8 (unmodified crushed stone) had the highest. Normal strain in the X-X direction was also analyzed, with peak values shown in Fig. 3.

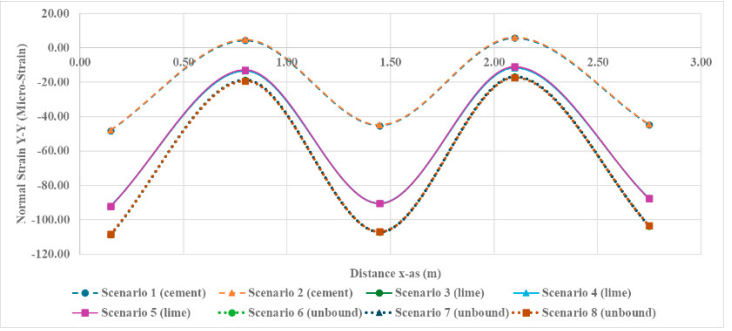

Fig. 2. Normal strains in Y-Y direction.

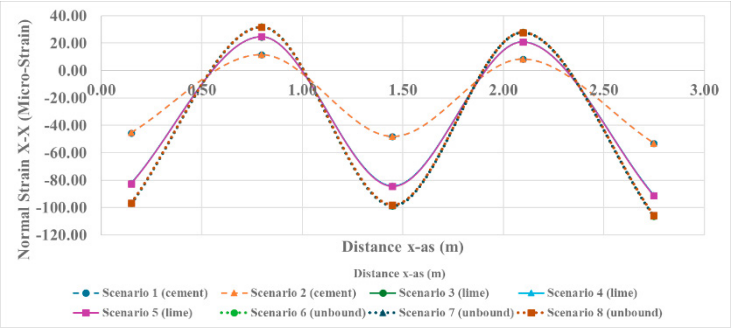

Fig. 3. Normal strains in X-X direction.

The division into three groups is clear. Comparing Fig. 2 and Fig. 3 shows that Group 1 values are similar in both directions, while Groups 2 and 3 show greater differences. Within all groups, strain varies most between tires, except in Group 1, where the most considerable difference is under tire 3. Absolute Y-Y strain values are generally higher than X-X beneath tires 1 and 2 and between tires, except under tire 3, where X-X is higher for all groups. Group 1 also shows higher X-X strain under tire 2. For Groups 1 and 2, the highest strain occurs in the X-X direction under tire 3; for Group 3, the maximum is the Y-Y strain under tire 1. Overall, surface layer type (SMA-C or ZOA-B) and thickness have a limited impact on fatigue resistance; the base layer is the main factor affecting fatigue behavior.

3.3. Empirical Models

As described earlier, the strain values obtained from the simulations were then used in empirical models. In the case of rutting, the empirical model was applied, as presented in Equation 2. Furthermore, it is essential to note that M1 refers to the point located midway between tire 1 and tire 2, while M2 corresponds to the point situated between tire 2 and tire 3. These positions were used as reference locations to evaluate the pavement structure strains. The resulting outcomes for each scenario are summarized and presented in Table 3. The results confirm the strong influence of base material on rutting resistance. Simulations show the truck's middle wheel track imposes the highest load. Cement-stabilized crushed stone performed best, with superior rutting resistance. While surface layer effects are smaller, variations still cause notable differences in allowable load repetitions, up to 700,000–750,000. Table 3 shows

scenario 1 with the highest predicted service life of 3.69E+07 load repetitions. Critical lowest values are highlighted in bold.

Table 3. Allowable number of load repetitions before rutting becomes critical based on Z-Z strains.

	X-Coord (m)	Y-Coord (m)	Scenario 1	Scenario 2	Scenario 3	Scenario 4	Scenario 5	Scenario 6	Scenario 7	Scenario 8
Tire 1	0.147856	0.147856	6.32E+07	6.19E+07	4.27E+07	4.31E+07	4.18E+07	3.69E+07	3.69E+07	3.82E+07
M1	0.797856	0.147856	8.65E+07	8.51E+07	6.92E+07	6.95E+07	6.82E+07	6.43E+07	6.43E+07	6.55E+07
Tire 2	1.447856	0.147856	**3.69E+07**	**3.61E+07**	**2.61E+07**	**2.63E+07**	**2.56E+07**	**2.31E+07**	**2.31E+07**	**2.39E+07**
M2	2.097856	0.147856	9.12E+07	8.97E+07	7.22E+07	7.25E+07	7.12E+07	6.69E+07	6.69E+07	6.82E+07
Tire 3	2.747856	0.147856	7.28E+07	7.14E+07	4.80E+07	4.83E+07	4.70E+07	4.12E+07	4.12E+07	4.26E+07

Fatigue analysis was also conducted, considering both the X and Y directions. Interestingly, the highest pavement stresses in the X direction were found under the third wheel track of the truck, whereas in the Y direction, they occurred under the first wheel track. This directional stress distribution significantly affects the pavement's fatigue behavior. An empirical model was also applied for fatigue, as shown in Equation 1. This analysis considered both the X-X and Y-Y directions. The predicted service lives for fatigue in the X-X and Y-Y directions are shown in Table 4, along with the lowest allowable load repetitions (i.e., critical values at specific locations under load) being bolded.

Table 4. Allowable number of load repetitions before fatigue becomes critical based on X-X and Y-Y strains.

			Allowable number of load repetitions based on X-X strains							
	X-Coord (m)	Y-Coord (m)	Scenario 1	Scenario 2	Scenario 3	Scenario 4	Scenario 5	Scenario 6	Scenario 7	Scenario 8
Tire 1	0.147856	0.147856	2.27E+07	2.31E+07	1.35E+06	1.36E+06	1.34E+06	6.19E+05	6.19E+05	6.37E+05
M1	0.797856	0.147856	1.63E+10	1.62E+10	4.28E+08	4.31E+08	4.20E+08	1.24E+08	1.24E+08	1.29E+08
Tire 2	1.447856	0.147856	1.73E+07	1.75E+07	1.21E+06	1.22E+06	1.20E+06	5.74E+05	5.74E+05	5.92E+05
M2	2.097856	0.147856	7.65E+10	7.69E+10	9.53E+08	9.54E+08	9.40E+08	2.35E+08	2.35E+08	2.43E+08
Tire 3	2.747856	0.147856	**1.09E+07**	**1.10E+07**	**8.36E+05**	**8.42E+05**	**8.25E+05**	**4.02E+05**	**4.02E+05**	**4.15E+05**
			Allowable number of load repetitions based on Y-Y strains							
Tire 1	0.147856	0.147856	**1.76E+07**	**1.81E+07**	**7.97E+05**	**7.98E+05**	**7.95E+05**	**3.64E+05**	**3.64E+05**	**3.71E+05**
M1	0.797856	0.147856	1.52E+12	9.50E+11	8.21E+09	7.62E+09	9.51E+09	1.60E+09	1.60E+09	1.38E+09
Tire 2	1.447856	0.147856	2.37E+07	2.47E+07	8.69E+05	8.68E+05	8.70E+05	3.88E+05	3.88E+05	3.93E+05
M2	2.097856	0.147856	4.34E+11	3.00E+11	1.63E+10	1.49E+10	1.94E+10	2.65E+09	2.65E+09	2.24E+09
Tire 3	2.747856	0.147856	2.50E+07	2.59E+07	1.02E+06	1.02E+06	1.02E+06	4.55E+05	4.55E+05	4.62E+05

4. Discussion of Results

4.1. Rutting

The highest vertical strains consistently occurred beneath the second wheel due to overlapping stresses from tire interaction. Greater tire spacing could reduce this overlap and consequently the peak strains. Cement-stabilized base layers (Scenarios 1 & 2) showed significantly lower strains than lime-stabilized (Scenarios 3–5) and unmodified crushed stone bases (Scenarios 6–8), confirming their higher stiffness and superior resistance to permanent deformation. These findings align with Souliman et al. (2020), who also highlighted the effectiveness of base stabilization in reducing rutting. Regarding allowable load repetitions for rutting, Scenario 1 slightly outperformed Scenario 2, with 3.69E+07 versus 3.61E+07 repetitions, respectively. This minor advantage could be attributed to the higher stiffness modulus of the SMA-C surface layer used in Scenario 1 compared to the ZOA-B layer in Scenario 2, potentially improving stress distribution and reducing strain at the subgrade. Nonetheless, both scenarios significantly outperformed all other configurations, reinforcing that cement stabilization of the base layer is the key driver of enhanced rutting resistance, even when combined with relatively thinner asphalt layers (2×6 cm APO-A).

4.2. Fatigue Cracking

Fatigue cracking was evaluated by measuring horizontal normal strains at the bottom of the asphalt layer in both X–X and Y–Y directions. A clear grouping based on base type was observed: cement-stabilized bases demonstrated the lowest strain magnitudes, indicating superior fatigue resistance. Higher strain values correlate with increased fatigue sensitivity. Directional strain variations were notable; Y–Y strains peaked under the first and second tires, while X–X strains were highest under the third tire, reflecting complex stress states due to lateral load transfer and tire configuration. Surface layer types (SMA-C vs. ZOA-B) and thickness had only minor effects on fatigue strains, confirming that base layer composition remains the dominant factor controlling fatigue behavior. However, both cement-stabilized scenarios (1 & 2) performed very similarly and consistently better than the lime-stabilized (Scenarios 3–5) and unbound crushed stone bases (Scenarios 6–8). Scenario 2 achieved the highest allowable load repetitions in the Y–Y (1.81E+07) and X–X directions (1.10E+07).

4.3. Influence of Layer Thickness and Base Material

All scenarios had the same total pavement thickness of 80 cm, ensuring a consistent reference depth for strain measurements at the top of the subgrade. Despite uniform total thickness, differences in the surface layer thickness and type influenced performance, but to a lesser extent than base composition. Scenarios 1 and 2 featured the thinnest asphalt layers (2×6 cm APO-A) yet showed superior rutting and fatigue performance. In contrast, lime-stabilized bases (Scenarios 3–5) had thicker asphalt layers (up to 8 cm APO-A) but only moderate performance, indicating that increasing surface thickness cannot fully compensate for lower base stiffness. The unbound crushed stone bases (Scenarios 6–8), despite having the thickest asphalt layers (up to 2×8 cm APO-A), performed the worst. This confirms that base layer type plays a more critical role than surface layer thickness in overall structural performance under heavy repeated loading.

4.4. Service Life Estimation via Empirical Model Integration

Strain results were used in empirical models to estimate pavement service life. Cement-stabilized bases showed significantly longer service lives, about 40% higher rutting resistance than lime-stabilized and 54% higher than unbound crushed stone. Fatigue life improvements were even greater, with cement stabilization providing 16.5 to 36 times longer life than the other bases. Surface layer type and thickness had a smaller but noticeable effect, adding around 700,000 to 750,000 load repetitions to rutting life. These results highlight the dominant role of base composition in durability, with surface layers offering secondary benefits.

5. Conclusion

- Cement-stabilized base layers significantly enhance pavement resistance to rutting and fatigue cracking, outperforming lime-stabilized and unmodified crushed stone bases. Empirical model predictions aligned closely with strain-based assessments, with scenario 1 showing the most robust performance in all aspects.
- The allowable number of load repetitions indicates that fatigue life is significantly more affected by changes in base layer composition than by rutting performance.
- While surface layer composition and thickness have a measurable effect, their impact is minor compared to the base layer material. Nonetheless, material selection can influence the number of allowable repetitions by up to 750,000, underlining its non-negligible role.
- The second wheel consistently induces the highest vertical strain, suggesting a critical zone for rutting development.
- Horizontal strain distributions vary with wheel position and direction, affecting fatigue performance differently across the pavement surface.

While the numerical models provide valuable insights into pavement behavior under heavy truck loading, several limitations must be acknowledged. Temperature fluctuations, moisture infiltration, and seasonal effects were not

included, though these factors can significantly alter asphalt stiffness and base layer performance over time. Future work should incorporate viscoelastic material modeling to account for time- and temperature-dependent behavior, as well as hygrothermal effects that influence long-term rutting and fatigue.

Additionally, this study applied a static analysis and excluded the influence of vehicle dynamics, such as suspension effects and load transients due to braking or acceleration. Incorporating dynamic simulations could yield a more realistic representation of traffic loading. The assumption of a single triple-axle configuration limits the generalizability of the results. Future research should examine various axle types, tire pressures, and wander patterns.

This study also focused exclusively on Flemish Class B6 roads, representing regional networks. Future research could explore higher road classes (e.g., motorways) and their specific design requirements and material specifications to expand applicability. From a practical perspective, the findings offer valuable guidance for road authorities. The clear performance differences between base materials show that cement-stabilized crushed stone provides significantly better resistance to rutting and fatigue. This supports policy decisions that promote mechanically stabilized base layers, especially in regions with high truck volumes. Moreover, the scenario-based comparison can be used as a practical tool when choosing the right combination of layers for flexible pavements. The results help identify which materials and layer configurations lead to better performance. Despite the simplifications in the model, the study offers a solid and valuable foundation for designing road structures that are more durable, cost-efficient, and sustainable.

References

Agentschap Wegen en Verkeer. (2019). *Standaardbestek 250 voor de wegenbouw: Hoofdstuk 6 - Verharding*. Retrieved from https://wegenenverkeer.be/sites/default/files/uploads/documenten/Hoofdstuk06.pdf

Agentschap Wegen en Verkeer. (2023). *Vademecum standaardstructuren, versie 2023*. Retrieved from https://wegenenverkeer.be/sites/default/files/uploads/documenten/Vademecum%20Standaardstructuren%202023.pdf

Asim, M., Ahmad, M., Alam, M., Ullah, S., Iqbal, M. J., & Ali, S. (2021). Prediction of rutting in flexible pavements using finite element method. *Civil Engineering Journal, 7*(8), 1310–1326. https://doi.org/10.28991/cej-2021-03091727

Behiry, A. E. A. E.-M. (2012). Fatigue and rutting lives in flexible pavement. *Ain Shams Engineering Journal, 3*(4), 367–374. https://doi.org/10.1016/j.asej.2012.04.008

Yeganeh, A., Vandoren, B., & Pirdavani, A. (2023). Pavement rutting performance analysis of automated vehicles: contribution of flexible pavement layers' characteristics. *Road Materials and Pavement Design*, *25*(7), 1618–1629. https://doi.org/10.1080/14680629.2023.2268728

Devree, J. (2025). Asfalt, zoab. Retrieved from https://www.joostdevree.nl/shtmls/asfalt.shtml#:~:text=Steenmastiekasfalt%20(SMA)%20is%20een%20ZOAB,voor%20lokale%20en%20provinciale%20wegen

Elnashar, G., Bhat, R. B., & Sedaghati, R. (2019). Modeling pavement damage and predicting fatigue cracking of flexible pavements based on a combination of deterministic method with stochastic approach using Miner's hypothesis. *SN Applied Sciences, 1*(3). https://doi.org/10.1007/s42452-019-0238-5

Kumar, Y., Trivedi, A., & Shukla, S. K. (2024). Damage evaluation in pavement-geomaterial system using finite element-scaled accelerated pavement testing. Transportation Infrastructure Geotechnology, 11, 922-933. https://doi.org/10.1007/s40515-023-00309-y

Liu, Z., Zhang, L., Gao, Y., Dong, Y., Liu, Y., & Li, B. (2025). Mechanical Response and Fatigue Life Analysis of Asphalt Pavements Under Temperature-Load Coupling Conditions. Applied Sciences, 15(13), 7441. https://doi.org/10.3390/app15137441

Pavement Tools Consortium. (2025). PCC pavement. *Pavement Interactive*. Retrieved from https://pavementinteractive.org/reference-desk/pavement-types-and-history/pavement-types/pcc-pavement/

Pirdavani, A., Bunjong, S., Coenen, D., & Nulens, J. (2023). Analytical assessment of the impact of material properties on the performance of flexible and composite highway pavements in Flanders. *Transportation Research Procedia, 73*, 118–125. https://doi.org/10.1016/j.trpro.2023.11.899

Indian Roads Congress. (2018). *IRC:37-2018: Guidelines for the design of flexible pavements* (4th Rev.). New Delhi, India: Indian Roads Congress. Retrieved from https://nepalindata.com/media/resources/bulk_file/GUIDELINES%20FOR%20THE%20DESIGN%20OF%20FLEXIBLE%20PAVEMENTS%20%28Fourth%20Revision%29%2C%202018.pdf

Souliman, M. I., Bastola, N. R., & Zeiada, W. A. (2020). Improvement of fatigue and rutting performance with different base treatments. Material Science & Engineering International Journal, 4(5). https://doi.org/10.15406/mseij.2020.04.00138

Transport's Friend. (2025). Construction & use regulations vehicle axles. Retrieved from https://www.transportsfriend.org/construction-use-regulation/vehicle-axles/

Ullah, A., Pei Wen, B. H., Ullah, Z., Ali, B., & Khan, D. (2024). Evaluation of high modulus asphalts in China, France, and USA for durable road infrastructure, a theoretical approach. Retrieved from https://www.sciencedirect.com/science/article/pii/S095006182401763X